Avicenna J Environ Health Eng. 2016 June; 3(1):e7789. doi: 10.17795/ajehe-7789.

Published online 2016 June 28. **Research Article**

Synthesis of DNPH/SDS/Fe_3O_4 Nanoparticles for Removal of Cr (VI) Ions From Aqueous Solution

Soheil Sobhanardakani,[1,*] Raziyeh Zandipak,[2] and Mehrdad Cheraghi[1]

[1]Department of the Environment, College of Basic Sciences, Hamedan Branch, Islamic Azad University, Hamedan, Iran
[2]Young Researchers and Elite Club, Hamedan Branch, Islamic Azad University, Hamedan, Iran

[*]*Corresponding author*: Soheil Sobhanardakani, Department of the Environment, College of Basic Sciences, Hamedan Branch, Islamic Azad University, Hamedan, Iran. Tel: +98-8134494170, Fax: +98-8134494170, E-mail: s_sobhan@iauh.ac.ir

Received 2016 April 30; **Revised** 2016 May 15; **Accepted** 2016 May 30.

Abstract

In this study, sodium dodecyl sulfate (SDS) coated magnetite modified with 2, 4-Dinitrophenylhydrazine was used to remove Cr (VI) ions from aqueous solution. The modified magnetite nanoparticles were characterized by X-ray diffraction (XRD) analysis, Fourier transform infrared spectroscopy (FT-IR), scanning electron microscopy (SEM), and SEM-EDXS measurement. The synthesized nanoparticles exhibited a high surface area of 75.5 m^2 g^{-1} and were of 20 - 35 nm in particle size. The effects of parameters, including pH, dose of adsorbent, temperature and contact time were investigated to find the optimum adsorption conditions. Adsorption data fits well with the Langmuir isotherm model with a maximum adsorption capacity (q_m) and a Langmuir adsorption equilibrium constant (b) of 169.5 mg g^{-1} and 0.168 L mg^{-1}, respectively. The adsorption kinetic agrees well with pseudo-second-order model.

Keywords: Adsorption, Chromium, Magnetite Nanoparticles, 2, 4-Dinitrophenylhydrazine

1. Introduction

With the rapid development of modern industry, the discharge of heavy metals such as chromium is an ecological threat, even at low concentration (1). Chromium occurs predominantly in trivalent Cr (III) and hexavalent Cr (VI) states in the natural environment. Cr (VI) is believed to be much more toxic than Cr (III) even at trace levels as it is considered to be carcinogenic and mutagenic (2). Cr (VI) ions are widely used in leather tanning, electroplating, cement manufacturing and dye industries (3, 4). Cr (VI) ions are highly soluble and mobile in aquatic system and often discharged into the environment at levels well above the regulatory trace limits leading to negative impacts on plants, animals and human health (5, 6). The U.S. environmental protection agency regulations set the maximum total Cr content in the drinking water as 0.1 mg L^{-1} (7). Therefore, more attention should be paid to the research on eliminating Cr (VI) from water to protect public health (8). Various methods are used to remove Cr (VI) ions, including adsorption, chemical precipitation, ion-exchange, electrochemical treatments, and membrane filtration (9, 10). Most of these methods have limitations because of high capital investment, operating costs, and ineffectiveness in meeting the environmental regulations (11). Adsorption technique is widely used to remove toxic heavy metal ions from the water, using different adsorbents (12).

Nano-oxides have been attracting much interest due to their potential applications and unique properties. For example, magnetite nanoparticles (Fe_3O_4) have attracted much attention for heavy metals removal because of high dispersibility, excellent magnetic responsivity, relative large surface area and ease of surface modification (13, 14).

However, the basic disadvantage of these adsorbents is the lack of selectivity in the removal of metal ions, which leads to other species interfering with the target metal ions (15). To overcome this problem, chemical or physical modification of the adsorbent surface with some organic compounds, especially chelating ones, is usually used to load the surface with some donor atoms such as oxygen, sulfur, nitrogen, and phosphorus (16). These donor atoms are capable of selective binding with certain metal ions. When a modifier is immobilized at the surface of the adsorbent, the target metals are not only removed by adsorption on the surface of the metal oxide, but could be removed by a surface attraction/ chemical bonding phenomenon on the newly added chemicals (17).

In this study, we used sodium dodecyl sulfate (SDS), an anionic surfactant, which tends to interact with the surface of magnetite nanoparticles and coats them. The con-

centration of SDS was fixed at 5×10^{-3} M, which is below the critical micellization concentration (c. m. c.) of SDS (8×10^{-3} M). Above the c. m. c., the excess of SDS would form micelles in the aqueous solution, which does not become adsorbed on the magnetite surface. The SDS can form hemimicelles or ad-micelles on the magnetite by strong adsorption (15). Afterwards, SDS-coated magnetite nanoparticles that were synthesized by a simple method, were modified with 2, 4-Dinitrophenlhydrazin (2, 4-DNPH is an important reagent which can act as electron pair donors, reacting with most of hard and intermediate cations), and used to remove Cr (VI) ions from water samples. The effects of pH, adsorbent dose, contact time and temperature on the adsorption efficiency were studied. Finally, kinetic and isotherm of adsorption were evaluated to determine the adsorption mechanism.

2. Materials and Methods

2.1. Apparatus and Reagents

All chemicals were of analytical grade available from Merck (Merck, Darmstadt, Germany) and used without further purification. Cr (VI) stock solutions were prepared by dissolving $K_2Cr_2O_7$ in double-distilled water. The solutions of different initial concentrations were prepared by diluting the stock solution in appropriate proportions.

The concentration of Cr (VI) ions was determined by inductively coupled plasma optical emission spectrometry (ICP-OES) (JY138 ultrace, France). All pH measurements were made with a 780 pH meter (Metrohm, Switzerland) combined with a glace-calomel electrode. The crystal structure of synthesized materials was determined by an XRD (38066 Riva, d/G.Via M. Misone, 11/D (TN) Italy) at ambient temperature. The structure of the nanoparticles was characterized by a scanning electron microscope (SEM-EDX, XL30 and Philips, the Netherlands). The elemental analysis was measured by scanning electron microscope energy dispersive X-ray spectroscopy (SEM-EDX, XL 30 and Philips, the Netherlands). FT-IR spectra (4000 - 400 cm^{-1}) in KBr were recorded on Perkin Elmer, spectrum 100, and FT-IR spectrometer. Specific surface area and porosity were defined by N_2 adsorption-desorption porosimetry (77 K), using a porosimeter (Bel Japan, Inc.).

2.2. Preparation of the Magnetite Modified with 2, 4-Dinitrophenylhydrazine (DNPH/SDS/Fe3O4 Nanoparticles)

The magnetite nanoparticles were prepared by the conventional co-precipitation method with minor modifications. $FeCl_3.6\ H_2O$ (11.68 g) and $FeCl_2.4\ H_2O$ (4.30 g) were dissolved in 200 mL double-distilled water under nitrogen gas atmosphere with vigorous stirring at 85°C, which led to smaller and more homogenized particles. Then, 20 mL of 30% NH_3 was added to the solution. After the addition the of NH_3 solution, the color of bulk solution was changed from orange to black immediately. The magnetite precipitates were washed twice with double-distilled water, and once with 0.02 mol L^{-1} sodium chloride and were separated from the solution with a magnet (18). Subsequently, 2.0 g sample of magnetite nanoparticles was suspended in 50 mL of water and mixed with 100 mg of SDS. Then, 20 mL of the solution of 2, 4-Dinitrophenylhydrazine (0.90 g 2, 4-Dinitrophenylhydrazine in concentrated HCl + acetonitril) was added. The suspension was stirred at 60°C for three hours. The mixture was followed by evaporation of the solvent, washing, air-drying, and storing in a closed bottle for subsequent use.

2.3. Point of Zero Charge pH (pHPZC)

The point of zero charge (PZC) is a characteristic of metal oxides (hydroxides) and of fundamental importance in surface science. It is a concept relating to the phenomenon of adsorption, and describes the condition when the electrical charge density on a surface is zero. In this study, the pH_{PZC} of the DNPH/SDS/Fe_3O_4 nanoparticles was determined in degassed 0.01 mol L^{-1} $NaNO_3$ solution at 20°C. Aliquots of 30 mL 0.01 mol L^{-1} $NaNO_3$ were mixed with 0.05 g DNPH/SDS/Fe_3O_4 nanoparticles in several beakers. The pHs of the solutions were adjusted at a range of 2.0 - 9.0, using 0.01 mol L^{-1} of HNO_3 and/or NaOH solutions as appropriate. The initial pHs of the solutions were recorded, and the beakers were covered with parafilm and shaken for 24 hours. The final pH values were recorded, and the pH_{pzc} is the point where the $pH_{initial} = pH_{final}$ (18).

2.4. Batch Adsorption Experiments

Adsorption experiments were carried out by adding 0.05 g of DNPH/SDS/Fe_3O_4 nanoparticles to a 25 mL conical flask, containing 10 mL of Cr (VI) solution at the temperature of 25°C. The initial Cr (VI) concentrations varied from 50 to 500 mg L^{-1}. The pH of the solution was adjusted to 2 - 9, using 0.1 mol L^{-1} HCl and/or 0.1 mol L^{-1} NaOH solutions. Then, the flasks were transferred to a thermostatic shaker, and shaken at 150 rpm for 24 hours. Then metal loaded magnetite nanoparticles were separated with magnetic decantation, and the residual concentration of Cr (VI) ions in the bulk (C_e) was determined, using an ICP-OES analysis. The concentration of the Cr (VI) ions remained in the adsorbent phase (q_e, mg g^{-1}) was calculated using the following formula:

Equation 1.

$$q_e = \frac{(C_o - C_e) \times V}{W} \quad (1)$$

Where C_0 and C_e (mg L^{-1}) are initial and equilibrium concentrations, respectively; V (L) is the volume of solution and W (g) is the mass of adsorbent.

Finally, the Cr (VI) ions removal efficiency was calculated using the following formula:

Equation 2.

$$R\,(\%) = \frac{C_o - C_e}{C_o} \times 100 \quad (2)$$

3. Results and Discussion

3.1. Characterization of Modified Magnetite Nanoparticles

The SEM image of the nanoparticles revealed that the average diameter for DNPH/SDS/Fe_3O_4 nanoparticles was around 20 - 35 nm with a spherical shape (Figure 1A). Figure 1B shows a typical SEM-EDX elemental analysis of SDS-coated magnetite nanoparticles. From the peak area of Fe and S, the atomic ratio of Fe/S is obtained to be 96.66/3.34 = 28.9, indicating the surface SDS coverage ratio of Fe_3O_4 nanoparticles. Perhaps, a near monolayer of the surface coating is due to the incompleteness of surface protonation and existence of the spatial resistance for the surface coating reaction.

The X-ray diffraction pattern of Fe_3O_4 nanoparticles is demonstrated in Figure 2. Furthermore, all the diffraction peaks were consistent with the six diffraction peaks at (220), (311), (400), (422), (511) and (440), compared with the joint committee on powder diffraction standards (JCPDS card, file No. 79 - 0418), which are indexed to the cubic spinel phase of Fe_3O_4. Therefore, the obtained XRD pattern indicates that the prepared nanoparticles are Fe_3O_4. The average crystallite size (D in nm) of Fe_3O_4 was determined from XRD pattern according to the Scherrer formula.

$$D = \frac{K\lambda}{\beta cos\theta} \quad (3)$$

where λ is the wavelength of the X-ray radiation (1.5406 Å), K is a constant taken as 0.89, θ is the diffraction angle, and β is the full width at half maximum (FWHM). The average size of the Fe_3O_4 was calculated as around 22 nm.

The FT-IR spectra of 2, 4-DNPH (A), Fe_3O_4 nanoparticles (B) and DNPH/SDS/Fe_3O_4 nanoparticles (C) are shown in Figure 3. The peak at 580 cm^{-1} corresponds to Fe–O bond in Fe_3O_4 (Figure 3B). After modifying the magnetite with 2, 4-DNPH, the modified magnetite nanoparticles showed a visible broad band in the 3200 - 3500 cm^{-1} region, which was due to stretching the vibrations of OH or N–H groups with varying degrees of H bonding. The absorption spectrum revealed that the absorption bands at 1345 cm^{-1}, 1532 cm^{-1} and 1598 cm^{-1} correspond to the bending vibration of N–H group (Figure 3C). Comparison of these characteristic spectral bands indicated that the surface modified magnetite nanoparticles contained –NH–functional group as a result of the immobilization procedure.

Specific surface areas are commonly reported as BET surface areas obtained by applying the theory of Brunauer, Emmett, and Teller (BET) to nitrogen adsorption/desorption isotherms measured at 77 K. This is a standard procedure to determine the specific surface area of the sample. The specific surface area of the sample is determined by the physical adsorption of a gas on the surface of the solid, and by measuring the amount of the adsorbed gas corresponding to a monomolecular layer on the surface. The data were treated according to the BET theory (19, 20). The results of the BET method revealed that the average specific surface areas of Fe_3O_4 nanoparticles and DNPH/SDS/Fe_3O_4 nanoparticles were 99.3 and 75.5 m2 g^{-1}, respectively. Considering these values, it can be concluded that the synthesized nanoparticles have relatively large specific surface areas. This decrease in the surface area of DNPH/SDS/Fe_3O_4 nanoparticles, as compared to Fe_3O_4 nanoparticles, is possibly due to aggregation after surface modification.

3.2. Effect of Solution pH

The solution pH is an important operational parameter in the adsorption process, because it affects the solubility of the metal ions, concentration of the counter ions on the functional groups of the adsorbent, and the degree of ionization of the adsorbent during reaction. To study the effect of pH on Cr (VI) adsorption, the pH of the solution in the adsorption experiment was varied between 2 and 9 by adjusting with HCl/NaOH. The point of zero charge (pH_{pzc}) value determined for DNPH/SDS/Fe_3O_4 nanoparticles was 5 (Figure 4A). The effect of pH on the adsorption of Cr (VI) ions on DNPH/SDS/Fe_3O_4 nanoparticles is illustrated in Figure 4B. The value of Cr (VI) removal percentage reached a maximum at pH 4 and decreased sharply.

The explanation would be addressed as the pH of the aqueous solution affects the stability of chromium speciation and the surface charge of the adsorbent. At pH 2, the chromium ions exist in the form of H_2CrO_4, while in the pH range of 2 - 9, different forms of chromium, such as $Cr_2O_7^{2-}$, $HCrO_4^-$, and $Cr_3O_{10}^{2-}$, coexist, although $HCrO_4^-$ predominates. As the pH increases, those form shifts to $Cr_2O_4^{2-}$ and $Cr_2O_7^{2-}$. Cr (VI) exist predominantly as $HCrO_4^-$ in aqueous solution below pH 5 ($pH < pH_{pzc}$), and the amino groups ($-NH_2$) of DNPH/SDS/Fe_3O_4 nanoparticles would be in protonated cationic form ($-NH_3^+$) to a higher extent in acidic solution. This results in the stronger attraction for negatively charged ions. Electrostatic interaction between the adsorbent and $HCrO_4^-$ ions also contributes to the high Cr (VI) removal. However, at the pH lower than 4, a decrease was observed in uptake capacity as the predomination of

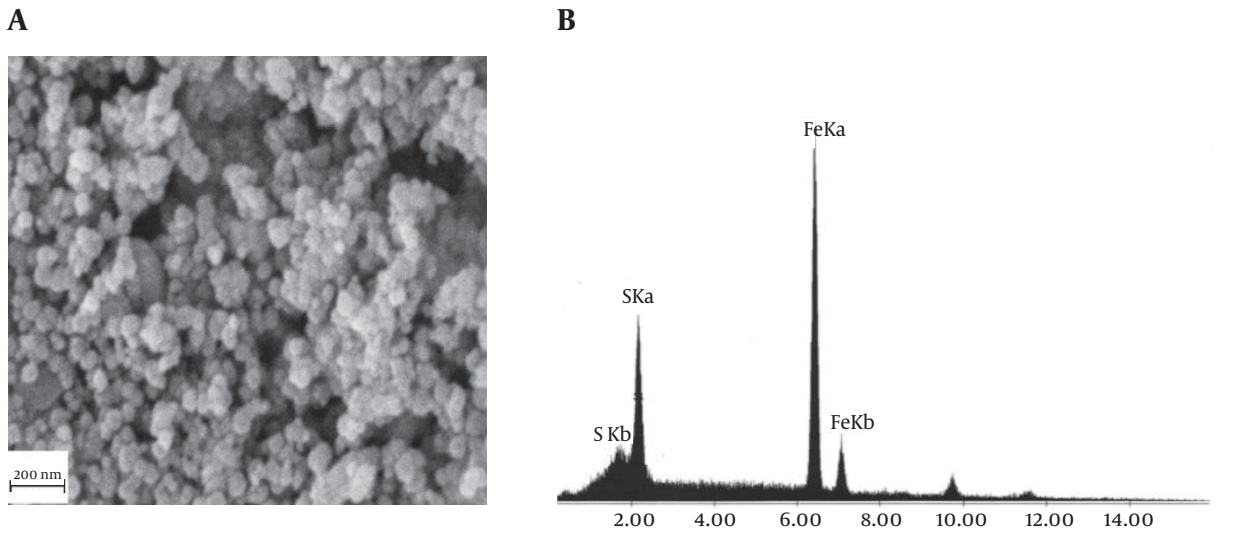

Figure 1. A, SEM Image of DNPH/SDS/Fe_3O_4 Nanoparticles; B, SEM-EDX Spectrum of SDS-Coated Magnetite Nanoparticles

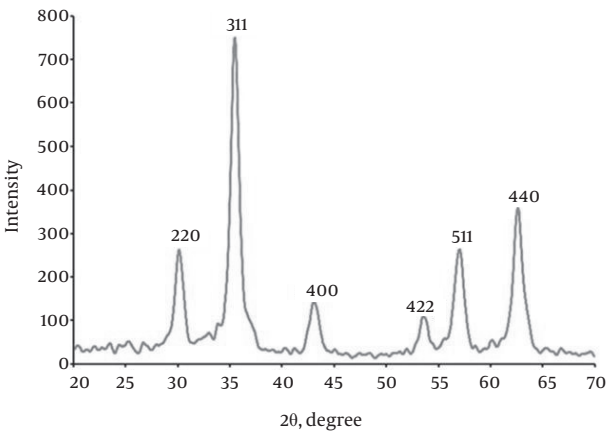

Figure 2. XRD Patterns of Fe_3O_4 Nanoparticles

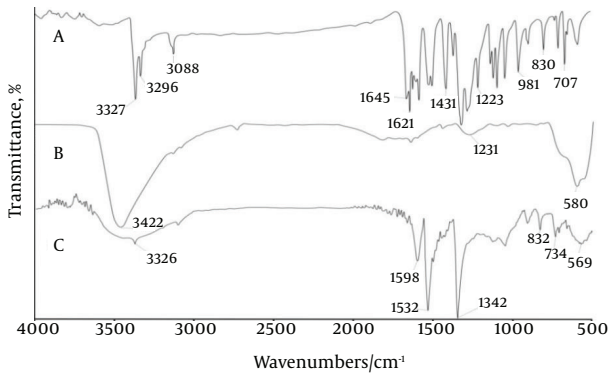

Figure 3. FT-IR Spectrum of the 2, 4-DNPH (A), Fe_3O_4 Nanoparticles (B) and DNPH/SDS/Fe_3O_4 Nanoparticles (C)

H_2CrO_4 and as the strong competition for adsorption sites between H_2CrO_4 and protons. The decreasing of the adsorption capacity at higher pH values may be explained by the dual competition of CrO_4^{2-} and OH^- for adsorption. Kim et al. (21) have found similar results.

3.3. Effect of Adsorbent Dose

To evaluate the correlation of Cr (VI) adsorption on adsorbent dose, various doses (0.01 - 0.07 g) of DNPH/SDS/Fe_3O_4 nanoparticles, at a temperature of 25°C, was added into 10 mL of 50 mg L^{-1} Cr (VI) solution. The relation between the adsorbent dose and removal percentage of Cr (VI) ions by the DNPH/SDS/Fe_3O_4 nanoparticles is shown in Figure 5. The removal percentage of Cr (VI) ions increased with rising the adsorbent dose due to an increase in the number of adsorption sites. As the adsorbent dose increased from 0.01 to 0.05 g, the removal efficiency of Cr (VI) ions increased significantly from 38% to 99.3%. However, the higher adsorbent dose results in a constant removal capacity of DNPH/SDS/Fe_3O_4 nanoparticles. It is believed that at the low adsorbent dose, the dispersion of DNPH/SDS/Fe_3O_4 nanoparticles in aqueous solution is better, that is, all of the active sites on the adsorbent surface are entirely uncovered, which could accelerate the approachability of Cr (VI) molecules to a large number of the adsorbent active sites. Thus, the adsorption on the surface active sites is saturated quickly, performing a high re-

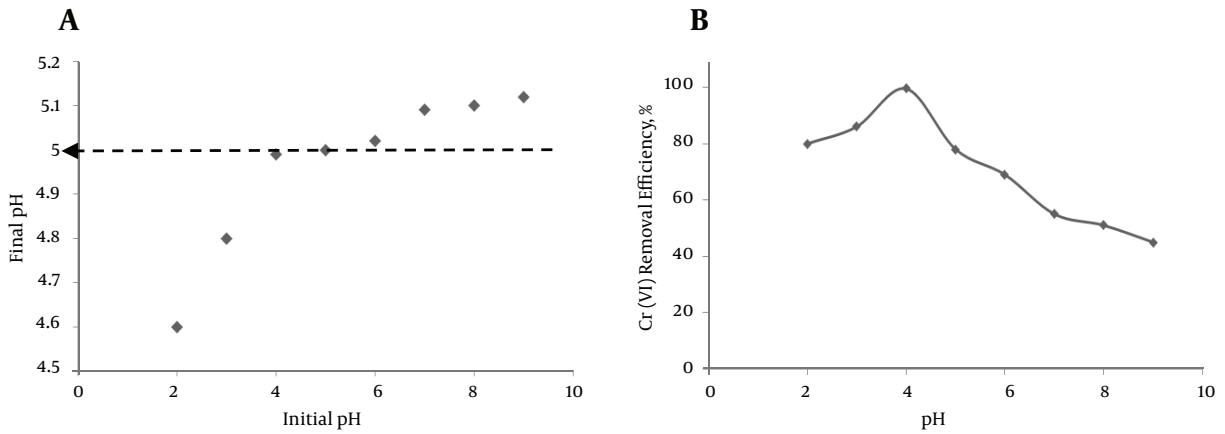

Figure 4. (A) pH Variation in Terms of Initial pH of Solution to Determine the Point of Zero Charge pH. (B) Effect of Solution pH on the Removal Percentage of Cr (VI) Ions by DNPH/SDS/Fe_3O_4 Nanoparticles

moval capacity. Similar results were observed by Wu (2016), who investigated the effect of the dose of adsorbent on the removal of Cr (VI) ions from aqueous solution by amine-functionalized modified rice straw, and indicated that adsorption increases with increasing the dose of adsorbent. Then, the removal efficiency remains unchanged with an increase in the adsorbent dose (22).

3.4. Effect of Temperature

To study the influence of temperature, experiments at 25°C, 35°C, 45°C and 55°C were accomplished, and the results are presented in Figure 6. It has been discovered that the adsorption process is more favorable at lower temperatures. This is mainly because of decreased surface activity, implying that adsorption between Cr (VI) ions and DNPH/SDS/Fe_3O_4 nanoparticles is an exothermal reaction. With increasing temperature, the attractive forces between the DNPH/SDS/Fe_3O_4 nanoparticles surface and Cr (VI) ions are weakened, and adsorption decreases. Similar phenomenon has also been shown in the adsorption of Cr (VI) ion from water with graphenes magnetic material (7).

3.5. The Effect of Contact Time and Adsorption Kinetic

The contact time between the adsorbate and adsorbent is the most important design parameter that affects the performance of adsorption processes. Figure 7 represents a plot of the removal efficiency of Cr (VI) versus contact time for various Cr (VI) concentrations. Obviously, Cr (VI) adsorption increases with contact time and gradually reaches equilibrium for all samples. A rapid adsorption is observed within 60 minutes in the availability of large number of vacant sites. Subsequently, the diminishing availability of the remained active sites and the decrease in the driving force lead to the slow adsorption process. Similar results were observed by Shi, who investigated the ef-

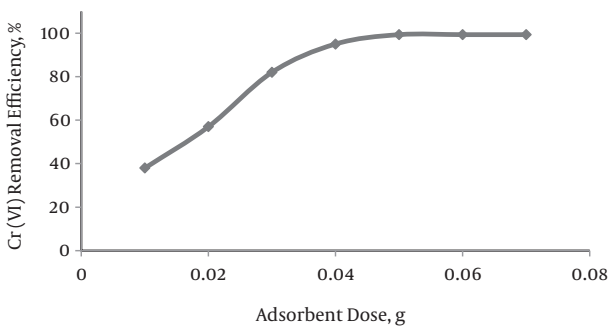

Figure 5. The Effect of Dose of DNPH/SDS/Fe_3O_4 Nanoparticles on the Removal Percentage of Cr (VI) ions

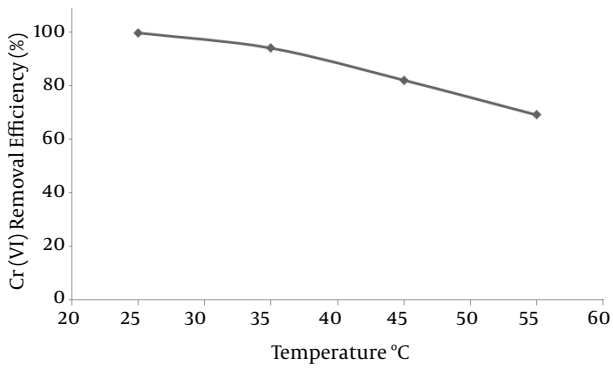

Figure 6. The Effect of Temperature on the Removal Percentage of Cr (VI) Ions

fect of contact time on the removal of Cr (VI) from aqueous solution by magnetite membranes, and indicated that adsorption increases with the increase in contact time (8).

To analyze the adsorption kinetics, pseudo-first-order and pseudo-second-order (23) models were used to describe the adsorption kinetic data, which can be expressed in the linear forms as follows:

$$\ln(q_e - q_t) = \ln(q_e) - \frac{k_1 t}{2.303} \quad (4)$$

$$\frac{t}{q_t} = \frac{1}{k_2 q_e^2} + \frac{t}{q_e} \quad (5)$$

where q_e and q_t are the amount of Cr (VI) ions adsorbed (mg g^{-1}) at equilibrium and time t (minute); k_1 is the rate constant of pseudo-first-order (minute^{-1}); k_2 is the rate constant of pseudo-second-order (g mg^{-1} minute^{-1}) for adsorption.

The adsorption kinetic plots are shown in Figure 8, and the related parameters calculated from the two models are listed in Table 1. The values of the correlation coefficients (R^2) clearly indicated that the adsorption kinetics closely followed the pseudo-second-order model rather than the pseudo-first-order model. Moreover, the calculated equilibrium adsorption capacity value, q_e, cal, was also closer to the experimental q_e, exp value. Therefore, it was reasonable to conclude that the rate-limiting step during the adsorption was chemisorption, which involved valence forces through sharing or exchanging electrons between the metal ion and the adsorbent.

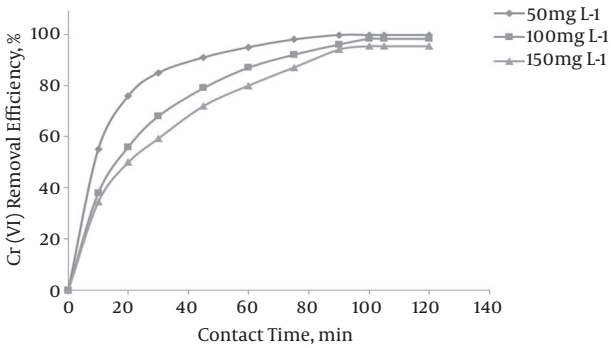

Figure 7. The Effect of Contact Time on the Removal Percentage of Cr (VI) Ions

3.6. Equilibrium Studies

The effect of initial Cr (VI) concentration on the adsorption efficiency of DNPH/SDS/Fe_3O_4 nanoparticles was investigated under the optimal pH value of 4 and fixed contact time of 90 minutes. Adsorption efficiency Cr (VI) ions gradually decreased with increasing initial Cr (VI) ions concentration, ranging from 50 to 500 mg L^{-1}. It has decreased to 68% when the initial Cr (VI) ions concentration was 500 mg L^{-1}.

The analysis of isotherm data is important to predict the adsorption capacity of the adsorbent, which is one of the main parameters required for the design of an adsorption system. Adsorption isotherm of Cr (VI) onto the DNPH/SDS/Fe_3O_4 nanoparticles was obtained at pH 4 with various initial Cr (VI) concentrations. The Langmuir Equation 6, Freundlich Equation 7, and Temkin Equation 8 were employed to fit the adsorption isotherms (24, 25):

Equation 6.

$$\frac{C_e}{q_e} = \frac{C_e}{q_m} + \frac{1}{q_m b_l} \quad (6)$$

Equation 7.

$$lnq_e = \frac{1}{n} lnC_e + lnk_f \quad (7)$$

$$q_e = Blnk_t + BlnC_e \quad (8)$$

Where c_e (mg L^{-1}) is the equilibrium concentration of Cr (VI) ions in solution, qe (mg g^{-1}) is the equilibrium adsorption capacity of DNPH/SDS/Fe_3O_4 nanoparticles, qm (mg g^{-1}) is the maximum adsorption capacity of DNPH/SDS/Fe_3O_4 nanoparticles for monolayer coverage, b (L mg^{-1}) is a constant related to the adsorption free energy, K_f ($mg^{1-(1/n)}$ $L^{1/n}$ g^{-1}) is a constant related to adsorption capacity, and n is an empirical parameter related to adsorption, K_t is the equilibrium binding constant (L mg^{-1}), corresponding to the maximum binding energy, and constant B is related to the heat of adsorption. The adsorption isotherms are presented in Figure 9. The adsorption constants obtained from the isotherms are listed in Table 2.

The calculated determination coefficient of the Langmuir model (R^2 = 0.995) was higher than that of the Freundlich and Temkin models, indicating that the Langmuir model better correlated with the adsorption isotherm, and could be used to describe the adsorption isotherms. Langmuir adsorption is reported as a reversible phenomenon, and the coverage is monolayer with finite adsorption sites. The maximum adsorption capacity (q_{max}) of Cr (VI) on the DNPH/SDS/Fe_3O_4 nanoparticles was calculated as 169.5 mg g^{-1} according to the Langmuir model, which was higher than other adsorbents listed in Table 3. In addition, the calculated RL was between 0 and 1, which further indicated that the adsorption isotherms obeyed the Langmuir model.

Table 1. Pseudo-First Order and Pseudo-Second Order Kinetic Model Parameters for the Adsorption of Cr (VI) Ions onto DNPH/SDS/Fe_3O_4 Nanoparticles at 25°C

		Pseudo-First-Order Kinetic model				Pseudo-Second-Order Kinetic		
	C_0 (mg L^{-1})	q_e exp (mg g^{-1})	q_{e1} (mg g^{-1})	k_1 (min^{-1})	R^2	q_{e2} (mg g^{-1})	k_2 (g mg^{-1} min^{-1})	R^2
Cr (VI)	50	25.93	8.679	0.040	0.617	26.02	0.004	0.999
	100	57.11	36.59	0.054	0.558	58.82	0.001	0.999
	150	88.5	53.51	0.053	0.547	90.90	0.000	0.998

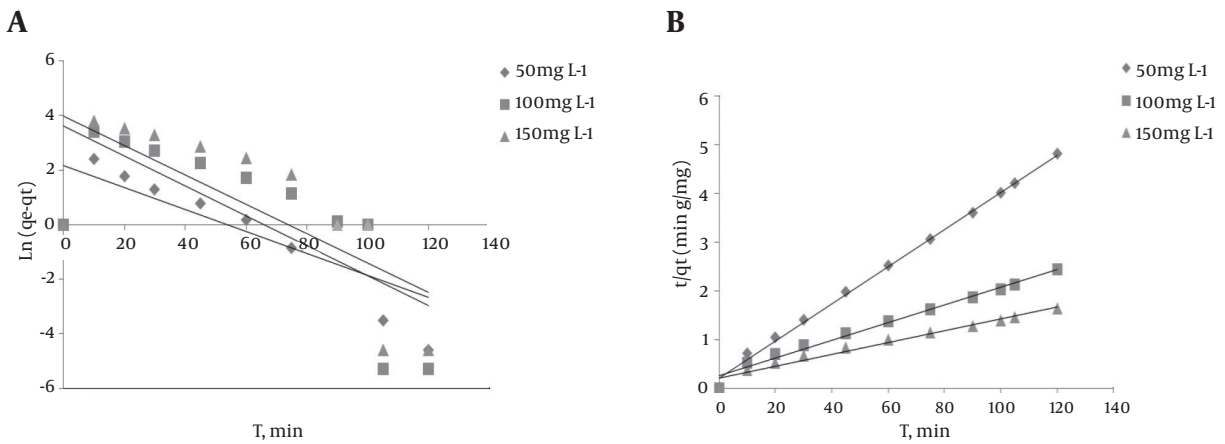

Figure 8. (A) Pseudo-First-Order Kinetic Plot, and (B) Pseudo-Second-Order Kinetic Plot for the Adsorption of Cr (VI) Ions onto DNPH/SDS/Fe_3O_4 Nanoparticles at 25°C

Table 2. Isotherm Parameters of Adsorption of Cr (VI) Ions onto DNPH/SDS/Fe_3O_4 Nanoparticles at 25°C

	Langmuir			Freundlich			Temkin		
b (L mg^{-1})	q_m (mg g^{-1})	R_L	R^2	K_f ($mg^{1-(1/n)}$ $L^{1/n}$ g^{-1})	n	R^2	K_T (L mg^{-1})	B	R^2
0.168	169.5	0.106	0.995	48.42	3.802	0.974	0.899	20.66	0.960

Table 3. Comparison of Adsorption Capacities of Cr (VI) with Other Adsorbents

Adsorbent	Maximum Adsorption Capacity (mg g^{-1})	Reference
Coconut tree sawdust	3.60	(26)
Multiwalled carbon nanotubes	4.2	(27)
Al (OH) CO_3	60	(28)
Activated carbon	36	(29)
Graphenes magnetic material	39.9	(7)
MnO_2 nanowires	152	(17)
DNPH/SDS/Fe_3O_4 nanoparticles	169.5	This work

4. Conclusion

In summary, we successfully synthesized DNPH/SDS/Fe_3O_4 nanoparticles to remove Cr (VI) ions from aqueous solutions. The results revealed that the optimized experimental parameters for Cr (VI) adsorption were pH 4, dose 0.05, contact time 90 minutes, initial concentration 50 mg L-1 and temperature 25°C. Moreover, the experimental results showed that about 99.5% of Cr (VI) ions were removed from aqueous solutions. The DNPH/SDS/Fe_3O_4 nanoparticles before and after the adsorption process

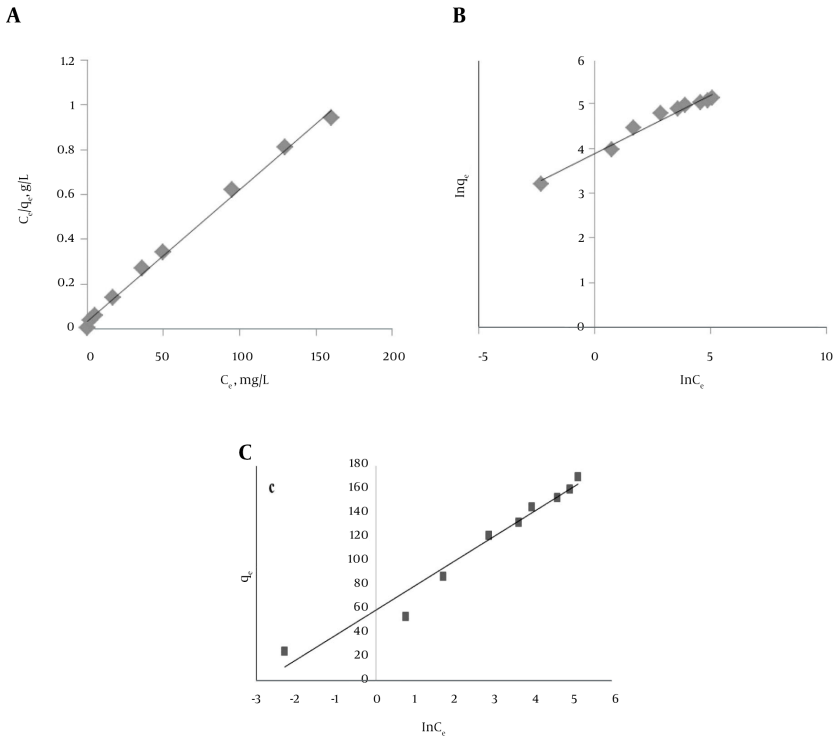

Figure 9. (A) Langmuir, (B) Freundlich and (C) Temkin Isotherms for Adsorption of Cr (VI) Ions onto DNPH/SDS/Fe_3O_4 Nanoparticles at 25°C

can be easily separated from the aqueous solution by the external magnetic field. The adsorption kinetics and adsorption isotherm showed that the adsorption kinetics could be modeled by the pseudo-second-order model and that the isotherm equilibrium data were well fitted with the Langmuir model.

Acknowledgments

The authors are grateful to the Hamedan Branch, Islamic Azad University for providing facilities to conduct and complete this study.

References

1. Lv G, Li Z, Jiang W, Ackley C, Fenske N, Demarco N. Removal of Cr (VI) from water using Fe (II)-modified natural zeolite. *Chem Eng Res Design.* 2014;**92**(2):384–90.
2. Kaprara E, Seridou P, Tsiamili V, Mitrakas M, Vourlias G, Tsiaoussis I, et al. Cu-Zn powders as potential Cr(VI) adsorbents for drinking water. *J Hazard Mater.* 2013;**262**:606–13. doi: 10.1016/j.jhazmat.2013.09.039. [PubMed: 24113648].
3. Ng IS, Wu X, Yang X, Xie Y, Lu Y, Chen C. Synergistic effect of Trichoderma reesei cellulases on agricultural tea waste for adsorption of heavy metal Cr(VI). *Bioresour Technol.* 2013;**145**:297–301. doi: 10.1016/j.biortech.2013.01.105. [PubMed: 23419991].
4. Liu Y, Liu Y, Hu X, Guo Y. Adsorption of Cr (VI) by modified chitosan from heavy-metal polluted water of Xiangjiang River, China. *Trans Nonferrous Met Soc China.* 2013;**23**(10):3095–103.
5. Melita L, Popescu M. Removal of Cr (VI) from industrial water effluents and surface waters using activated composite membranes. *J Mem Sci.* 2008;**312**(1):157–62.
6. Du Y, Zheng G, Wang J, Wang L, Wu J, Dai H. MnO 2 nanowires in situ grown on diatomite: Highly efficient absorbents for the removal of Cr (VI) and As (V). *Microporous Mesoporous Material.* 2014;**200**:27–34.
7. Guo X, Du B, Wei Q, Yang J, Hu L, Yan L, et al. Synthesis of amino functionalized magnetic graphenes composite material and its application to remove Cr(VI), Pb(II), Hg(II), Cd(II) and Ni(II) from contaminated water. *J Hazard Mater.* 2014;**278**:211–20. doi: 10.1016/j.jhazmat.2014.05.075. [PubMed: 25016452].
8. Shi M, Li Z, Yuan Y, Yue T, Wang J, Li R, et al. In situ oxidized magnetite membranes from 316L porous stainless steel via a two-stage sintering process for hexavalent chromium [Cr (VI)] removal from aqueous solutions. *Chem Eng J.* 2015;**265**:84–92.
9. Al-Zoubi H, Ibrahim K, Abu-Sbeih K. Removal of heavy metals from wastewater by economical polymeric collectors using dissolved air flotation process. *J Water Process Eng.* 2015;**8**:19–27.
10. Sobhanardakani S, Parvizimosaed H, Olyaie E. Heavy metals removal from wastewaters using organic solid waste-rice husk. *Environ Sci Pollut Res Int.* 2013;**20**(8):5265–71. doi: 10.1007/s11356-013-1516-1. [PubMed: 23381799].
11. Cui L, Wang Y, Gao L, Hu L, Yan L, Wei Q, et al. EDTA functionalized magnetic graphene oxide for removal of Pb (II), Hg (II) and Cu (II) in water treatment: Adsorption mechanism and separation property. *Chem Eng J.* 2015;**281**:1–10.
12. Ghaedi M, Biyareh M, Kokhdan S, Shamsaldini S, Sahraei R, Daneshfar A, et al. Comparison of the efficiency of palladium and silver nanoparticles loaded on activated carbon and zinc oxide nanorods loaded

on activated carbon as new adsorbents for removal of Congo red from aqueous solution: Kinetic and isotherm study. *Mater Sci Eng: C.* 2012;**32**(4):725–34.
13. Lai L, Xie Q, Chi L, Gu W, Wu D. Adsorption of phosphate from water by easily separable Fe3O4@SiO2 core/shell magnetic nanoparticles functionalized with hydrous lanthanum oxide. *J Colloid Interface Sci.* 2016;**465**:76–82. doi: 10.1016/j.jcis.2015.11.043. [PubMed: 26641568].
14. Turkmen M, Turkmen A, Tepe Y, Töre Y, Ates A. Determination of metals in fish species from Aegean and Mediterranean seas. *Food Chem.* 2009;**113**(1):233–7.
15. Afkhami A, Moosavi R. Adsorptive removal of Congo red, a carcinogenic textile dye, from aqueous solutions by maghemite nanoparticles. *J Hazard Mater.* 2010;**174**(1-3):398–403. doi: 10.1016/j.jhazmat.2009.09.066. [PubMed: 19819070].
16. Wang J, Zheng S, Shao Y, Liu J, Xu Z, Zhu D. Amino-functionalized Fe(3)O(4)@SiO(2) core-shell magnetic nanomaterial as a novel adsorbent for aqueous heavy metals removal. *J Colloid Interface Sci.* 2010;**349**(1):293–9. doi: 10.1016/j.jcis.2010.05.010. [PubMed: 20542278].
17. Du Z, Zheng T, Wang P, Hao L, Wang Y. Fast microwave-assisted preparation of a low-cost and recyclable carboxyl modified lignocellulose-biomass jute fiber for enhanced heavy metal removal from water. *Bioresour Technol.* 2016;**201**:41–9. doi: 10.1016/j.biortech.2015.11.009. [PubMed: 26630582].
18. Sobhanardakani S, Zandipak R. 2,4-Dinitrophenylhydrazine functionalized sodium dodecyl sulfate-coated magnetite nanoparticles for effective removal of Cd(II) and Ni(II) ions from water samples. *Environ Monit Assess.* 2015;**187**(7):412. doi: 10.1007/s10661-015-4635-y. [PubMed: 26050063].
19. Brunauer S, Emmett P, Teller E. Adsorption of gases in multimolecular layers. *J Am Chem Soci.* 1938;**60**(2):309–19.
20. Venkatesha TG, Viswanatha R, Nayaka YA, Chethana BK. Kinetics and thermodynamics of reactive and vat dyes adsorption on MgO nanoparticles. *Chem Eng J.* 2012;**198**:1–10.
21. Kim MK, Sundaram K, Iyengar G, Lee K. A novel chitosan functional gel included with multiwall carbon nanotube and substituted polyaniline as adsorbent for efficient removal of chromium ion. *Chem Eng J.* 2015;**267**:51–64.
22. Wu Y, Fan Y, Zhang M, Ming Z, Yang S, Arkin A, et al. Functionalized agricultural biomass as a low-cost adsorbent: Utilization of rice straw incorporated with amine groups for the adsorption of Cr (VI) and Ni (II) from single and binary systems. *Biochem Eng J.* 2016;**105**:27–35.
23. Azizian S. Kinetic models of sorption: a theoretical analysis. *J Colloid Interface Sci.* 2004;**276**(1):47–52. doi: 10.1016/j.jcis.2004.03.048. [PubMed: 15219428].
24. Langmuir I. The adsorption of gases on plane surfaces of glass, mica and platinum. *Am Chem Soci.* 1918;**40**(9):1361–403.
25. Freundlich H, Heller W. The Adsorption of cis- and trans-Azobenzene. *Am Chem Soci.* 1939;**61**(8):2228–30.
26. Selvi K, Pattabhi S, Kadirvelu K. Removal of Cr(VI) from aqueous solution by adsorption onto activated carbon. *Bioresour Technol.* 2001;**80**(1):87–9. [PubMed: 11554606].
27. Hu J, Chen C, Zhu X, Wang X. Removal of chromium from aqueous solution by using oxidized multiwalled carbon nanotubes. *J Hazard Mater.* 2009;**162**(2-3):1542–50. doi: 10.1016/j.jhazmat.2008.06.058. [PubMed: 18650001].
28. Zhong LS, Hu JS, Cao AM, Liu Q, Song WG, Wan LJ. 3D flowerlike ceria micro/nanocomposite structure and its application for water treatment and CO removal. *Chem Mater.* 2007;**19**(7):1648–55.
29. Cao CY, Cui ZM, Chen CQ, Song WG, Cai W. Ceria hollow nanospheres produced by a template-free microwave-assisted hydrothermal method for heavy metal ion removal and catalysis. *Phys Chem C.* 2010;**114**(21):9865–70.